A Model for the Kinetics of Homotypic Cellular Aggregation Under Static Conditions

Sriram Neelamegham,*# Lance L. Munn,*§ and Kyriacos Zygourakis*
*Department of Chemical Engineering and the Institute of Biosciences and Bioengineering, Rice University, Houston, Texas 77251-1892; #Section of Leukocyte Biology, Department of Pediatrics, Baylor College of Medicine, Houston, Texas 77030; and §Department of Radiation Oncology, Harvard Medical School, Boston, Massachusetts 02114 USA

ABSTRACT We present the formulation and testing of a mathematical model for the kinetics of homotypic cellular aggregation. The model considers cellular aggregation under no-flow conditions as a two-step process. Individual cells and cell aggregates 1) move on the tissue culture surface and 2) collide with other cells (or aggregates). These collisions lead to the formation of intercellular bonds. The aggregation kinetics are described by a system of coupled, nonlinear ordinary differential equations, and the collision frequency kernel is derived by extending Smoluchowski's colloidal flocculation theory to cell migration and aggregation on a two-dimensional surface. Our results indicate that aggregation rates strongly depend upon the motility of cells and cell aggregates, the frequency of cell-cell collisions, and the strength of intercellular bonds. Model predictions agree well with data from homotypic lymphocyte aggregation experiments using Jurkat cells activated by 33B6, an antibody to the β_1 integrin. Since cell migration speeds and all the other model parameters can be independently measured, the aggregation model provides a quantitative methodology by which we can accurately evaluate the adhesivity and aggregation behavior of cells.

INTRODUCTION

Cell-cell interactions play a very important role in regulating various processes in normal physiological function and during immune response such as leukocyte-endothelium interactions and cytotoxic T-cell activity (Clayberger et al., 1987; Springer, 1995). A better understanding of the adhesion processes between these cells will give us the ability to devise new methods to regulate these phenomena.

The study of homotypic aggregation under an optical microscope is a common method used by immunologists to study the role of various reagents in activating and modulating cell adhesion (Rothlein and Springer, 1986; Bednarczyk and McIntyre, 1990). Fig. 1 presents images obtained in our laboratory showing the time course of a typical homotypic aggregation experiment, where Jurkat cells (a lymphoblastoid T-cell line) were activated by 33B6, a monoclonal antibody to the β_1 integrin. Initially the cells were spread out uniformly on the well surface. During the course of the experiment they migrated on the tissue culture surface, colliding with other cells to form large, multilayered aggregates. A recently developed aggregation assay has allowed us to accurately measure aggregation kinetics and show that both the size and morphology of cell aggregates follow temporal evolution patterns that strongly depend upon the cell type and the activation protocol (Munn et al., 1993; Neelamegham and Zygourakis, in press). Such information, however, is not sufficient for distinguishing among the various important mechanisms that affect cellular aggregation.

For cellular systems like the one described above, we expect that the rate of aggregation will depend on 1) the rate of collision of cells and cell aggregates, and 2) the ability of the two colliding species to bind upon contact. Collision rates should be strong functions of the cell migration speed and the size of the aggregates. In turn, cell migration speed is governed mainly by its cytoskeletal activity (Oster, 1984; Bretscher, 1994) and by cell-surface interactions (Lauffenburger, 1989). The fraction of cell collisions resulting in adhesion gives the sticking probability, which depends on the concentration of surface receptors and their affinities for the ligands on the opposing species (Bell, 1978, 1979; Hammer and Lauffenburger, 1987). These parameters are affected both by the level of cell activation and by more subtle biological variables, such as the cell cycle and cell-surface interactions. They are probably also time dependent because of activation and down-regulation of adhesion processes.

The above points are sometimes overlooked by investigators analyzing cellular adhesion by monitoring aggregation, and this can lead to misinterpretation of the experimental data. For example, two systems may have similar aggregation kinetics, even though they have very different binding capabilities: a system with highly motile cells with low-affinity receptors may be indistinguishable from one with cells having low motility but high-affinity receptors. Comparisons among various aggregation experiments are further complicated because of difficulties in controlling other system parameters such as the initial cell density. To resolve these problems, kinetic models must be developed and applied to the analysis of experimental aggregation data.

Received for publication 30 May 1996 and in final form 8 October 1996.
Address reprint requests to Prof. K. Zygourakis, Department of Chemical Engineering, MS 362, Rice University, P.O. Box 1892, Houston, TX 77251-1892. Tel.: 713-527-8101, ext. 3509; Fax: 713-285-5478; E-mail: kyzy@rice.edu.

0006-3495/97/01/51/14 $2.00

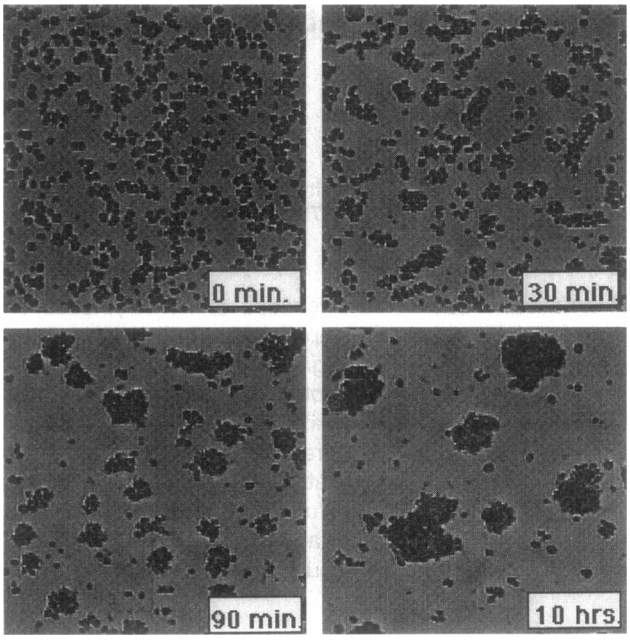

FIGURE 1 Homotypic aggregation. Digital images showing the temporal evolution of homotypic aggregates of Jurkat cells activated by a monoclonal antibody to the β_1 integrin, 33B6. Images were acquired at 0 min, 30 min, 90 min, and 10 h after mAb addition. Lymphocytes formed aggregates whose size and morphologies strongly depended on the cell type and the activation protocol.

Using the Smoluchowski equation (Smoluchowski, 1917) as a starting point, several investigators have developed macroscopic models to describe nonequilibrium aggregation events in a variety of biological and nonbiological fields, including polymer science, colloidal chemistry, and physics (Sutherland and Goodarx-nia, 1971; Zeichner and Schowalter, 1979; Botet and Jullien, 1984). In biological systems, Samsel and Perelson used the Smoluchowski approach to model the aggregation of erythrocytes into cylindrical clusters called "rouleaux" (Samsel and Perelson, 1982, 1984). More recently this method has been used by Dolgosheina et al. to study the agglutination of bacterial cells by bivalent antibodies (Dolgosheina et al., 1992). Several groups have also applied the Smoluchowski equation to simulate the aggregation and disaggregation kinetics of platelets (Nguyen and O'Rear, 1990; Huang and Hellums, 1993) and lymphocytes (Evans and Proctor, 1978).

In this paper we adapted Smoluchowski's colloidal flocculation theory (Smoluchowski, 1917) to model the kinetics of homotypic cellular aggregation under static conditions. To relax some of the restrictive assumptions of earlier models and to more accurately simulate the behavior of our aggregation system, we modified the kinetic kernel in accordance with our experimental findings and basic collision theory principles. Experimentally measured aggregation rates for Jurkat cells activated under various protocols agreed well with theoretical predictions. This comparison allowed us to quantify the dependence of aggregation rates on 1) the motility of cells and cell aggregates, 2) the frequency of cell-cell collision, and 3) a measure of the strength of intercellular bonds. Thus this model provides a potentially useful tool for identifying the important physiological parameters involved in aggregation and for correctly interpreting experimental data obtained from visual assays of homotypic cellular aggregation.

EXPERIMENTAL METHODS

Video microscopy and image-processing techniques were applied to measure the cell motility parameters and aggregation kinetics of Jurkat cells (a human lymphoblastoid T-cell line). These experiments were used to measure the mathematical model parameters and to compare experimental results with simulation predictions.

Aggregation measurements

We measured the aggregation kinetics of Jurkat cells (a human lymphoblastoid T-cell line) in RPMI media supplemented with fetal bovine serum (FBS) (Neelamegham et al., 1996; Neelamegham and Zygourakis, in press). Cells were seeded at a density between 1100 and 2000 cells/mm^2 in the video microscopy apparatus described earlier (Munn et al., 1993; Neelamegham and Zygourakis, in press). At the start of an aggregation experiment, cells were mainly found as singlets along with some doublets and a few small aggregates. During the course of the experiment, cell-cell collisions lead to the formation of larger multilayered cell aggregates, usually with considerable cell stacking (Fig. 1). A sequence of digital images was acquired at fixed time intervals (typically every 30 min for 8–10 h after activation) to monitor the aggregation kinetics.

An aggregation assay based on image processing was used to calculate the actual number of cells in each aggregate (Neelamegham and Zygourakis, in press). This allowed us to monitor the change in aggregate size distribution with time and the extent of cell stacking (i.e., the three-dimensional structure of aggregates). Aggregation kinetics was measured using the following indices.

Size indices

The extent of aggregation was quantified by monitoring the quartile values of the cell aggregate populations. The quartile values, Q_1, Q_2, and Q_3, are the aggregate sizes below which 25%, 50%, and 75%, respectively, of the cells are found.

Morphology index

The extent of stacking was quantified by the stacking index β, which is measured by monitoring the decrease in the cumulative projected area of the cells and cell aggregates during the aggregation experiment. The expression for the stacking index is

$$\beta = \frac{S_0 - S(t)}{S_0}, \tag{1}$$

where S_0 is the initial projected area of the cells and $S(t)$ is the projected area of the cells and the cell aggregates at time t. The stacking index depends on both the nature and dosage of the activating reagent. It is equal to zero if no three-dimensional aggregates are formed and all of the cells are in contact with the plate surface at all times. Low values of β (in the 0.1–0.2 range) indicate the formation of aggregates with some vertical stacking, whereas higher values in the 0.4–0.6 range indicate the presence of aggregates where 40–60% of the cells are stacked on top of other cells, forming large, multilayered clumps.

Cell migration measurements

Jurkat cells were maintained in RPMI-1640 (Sigma Chemical Co., St. Louis, MO) supplemented with 10% FBS (Sigma Chemical Co.). Before the experiment, the cells were washed twice in RPMI-1640 containing 10% FBS and carboxy methyl cellulose (CMC) (Sigma Chemical Co.) (Freshney, 1987). Addition of CMC increased the media viscosity from 1.32 centipoise to a value between 2.19 and 6.49 centipoises, depending on the CMC concentration. Increasing the viscosity is necessary for single-cell locomotion experiments to reduce the natural convection currents in the well (Bird et al., 1960) and to improve the quality of the data acquired. During the motility experiments the cell suspension was mixed with appropriate antibody and added to a 96-well tissue culture treated plate (Corning Glass Works, Corning, NY) maintained at 37°C and 5% CO_2 in a custom-built incubator placed on the motorized stage of a video microscope (Munn et al., 1993; Neelamegham and Zygourakis, in press). The cell seeding density was kept low at 17 cells/mm^2 to minimize cell-cell interactions and to allow us to study the motion of individual cells in a uniform environment.

Digital images were acquired at 10-min intervals using the National Institutes of Health Image 1.51 image-processing software (U.S. National Institutes of Health, available via anonymous ftp from zippy.nimh.nih.gov). A macro written in National Institutes of Health Image 1.51 was used to track the path of individual cells and to record the x, y coordinates of the center of the cell during the experiment (Neelamegham, 1995). The average locomotion speed S_k (in μm/h) for a population of N cells at any time was calculated from the discrete experimental observations using the formula

$$S_k = \frac{\sum_{i=1}^{N} |d_k|}{N\Delta t}, \tag{2}$$

where d_k is the displacement of the center of the cell in the interval Δt (between times t^{k-1} and t^k).

Cell migration was also modeled as a persistent random walk based on the Langevin equation (Doob, 1942; Dunn and Brown, 1987; Stokes et al., 1991). For random motility on a two-dimensional surface, the expected mean square displacement $\langle D^2 \rangle$ at time t is related to the root mean square speed S and the persistence time P by the equation

$$\langle D^2 \rangle = 2S^2P^2\left(\frac{t}{P} - 1 + e^{-t/P}\right). \tag{3}$$

A nonlinear regression procedure (NLIN procedure, SAS 6.07.02 package; Statistical Analysis System Institute, Cary, NC) was used to fit the experimentally measured mean square displacement at various times to the persistent random walk model (Eq. 3). To characterize the motion of the entire cell population, the random motility coefficient D was computed as follows (Alt, 1980; Farrell et al., 1990):

$$D = \frac{1}{2}PS^2. \tag{4}$$

The random motility coefficient D_i of aggregates with i cells was measured by analyzing the data from the aggregation experiments after the 6-h time point. At the 6-h time point, cell aggregates were identified and their paths were followed for the next 3 h. Since fewer than 10% of the aggregates were found to collide with other species in this 3-h time period, the aggregate size did not change substantially and the displacement measurements gave an accurate description of aggregate locomotion. The random motility coefficients of the aggregates were calculated using the random walk model for cell locomotion.

DEVELOPMENT OF THE MATHEMATICAL MODEL

We employed time-lapsed video recording to monitor the aggregation of various cell lines in the presence of monoclonal antibodies (Munn et al., 1993; Neelamegham and Zygourakis, in press). Viewing the experiment from time-lapsed tapes at 120× time compression, we saw actively crawling cells whose cytoskeletal activity did not subside when these cells aggregated (Neelamegham et al., 1996). Large cell aggregates also crawled over and between other cells, thus colliding with each other. The motion of aggregates was therefore driven by cellular activity.

These observations were used to formulate the appropriate assumptions for a model that describes cellular aggregation as a two-step process. Individual cells and cell aggregates move on a flat surface (e.g., bottom of tissue culture well) and collide with other cells or aggregates. These collisions may lead to the formation of larger cell aggregates (Fig. 1), which, in general, have a multilayered structure. This model considers collision of only two entities at a time and assumes that the system is closed (i.e., the total number of cells remains constant during the course of the experiment).

Basic modeling equations

We assume that each experiment starts with single cells placed in a well of area A_t. These singlets migrate and combine to form doublets, triplets, and larger aggregates. Let the maximum size of the aggregate that can be found in this system be N_0. If at any time t the total number of aggregates of size i ($i = 1, 2 \ldots N_0$.) in the well is n_i, then the concentration of aggregates of size i is

$$C_i = \frac{n_i}{A_t}. \tag{5}$$

The aggregation of cells is modeled as a set of reactions with multiple species based on Smoluchowski's collision theory (Chandrasekhar, 1943; Zeichner and Schowalter, 1979; Nguyen and O'Rear, 1990). The concentration of aggregates of a given size, C_i, during the course of an aggregation process can be found by solving the following system of ordinary differential equations:

$$\frac{dC_i}{dt} = \frac{1}{2}\sum_{j=1}^{i-1} k_{i-j,j}C_{i-j}C_j - \sum_{j=1}^{N_0-i} k_{i,j}C_iC_j + \sum_{j=i+1}^{N_0} b_{i,j}C_j - \frac{1}{2}\sum_{j=1}^{i-1} b_{j,i}C_i \quad \begin{matrix} i = 1, 2, 3 \ldots N_0 \\ j = 2, 3 \ldots N_0 \end{matrix}, \tag{6}$$

where $k_{i,j}$ is the rate constant for aggregate formation when two clumps of sizes i and j collide and adhere (in $\mu m^2 \cdot cells^{-1} \cdot h^{-1}$), $b_{i,j}$ is the disaggregation rate constant when a clump of size j breaks up and releases aggregates of sizes i and $(j - i)$ (in h^{-1}), and N_0 is the number of differential

equations that must be solved simultaneously (equal to the maximum aggregate size that can be formed in the system). The first term of Eq. 6 gives the rate at which aggregates of size i are formed by collision of aggregates of size j and $(i - j)$. The second term is the rate at which aggregates of size i disappear when these clumps collide with other aggregates of size j (i.e., all other sizes). The next two summations are due to the disaggregation or breakup of pre-existing clumps. The third term is the rate of formation of aggregates of size i when larger aggregates of size j break up, releasing two aggregates of size i and $(j - i)$. The last term is the rate of loss of aggregates when the clump of size i breaks up into smaller species. The first and the last terms are divided by 2 in order to avoid counting the contribution of these terms twice. Thus the overall mass balance of the system is satisfied. This system of ordinary differential equation must be solved subject to the initial conditions

$$C_i(t = 0) = \begin{cases} C_0 & i = 1 \\ 0 & i > 1 \end{cases}, \tag{7}$$

where C_0 is the initial cell seeding density (in singlets/mm^2).

For the lymphocyte systems studied in our laboratory, dissociation of aggregates was only observed on addition of an antagonist. In a few cases we observed the "ejection" of singlets from the aggregates, but this was a very rare event (e.g., approximately five cells might separate from aggregates over a typical 10-h experiment). In no experiments did we observe the breakup of a fully formed aggregate into two smaller aggregates, each containing more than one cell. For this reason, the third and fourth breakup terms in Eq. 6 have been dropped for all of the simulation results presented in this paper. However, the modeling equations can easily account for disaggregation in systems where such phenomena are important.

The aggregation rate constants

Solution of the above system of equations requires that we estimate the aggregation rate constants. Basic collision theory principles were combined with experimental observations to develop an expression for the rate constant for aggregate formation, k_{ij}. It is affected by two important factors: 1) the rate of collision, Z_{ij}, between aggregating species of size i and j and 2) the sticking probability, P_{ij} (i.e., the probability that the two clumps will adhere on collision). In analogy with collision theory, we define the rate coefficient kernel as

$$k_{ij}C_iC_j = Z_{ij}P_{ij}. \tag{8}$$

The collision frequency, Z_{ij}, depends on the rate at which the aggregating species diffuse on the well surface, their concentration, and their cross-sectional area during collision. The sticking probability, P_{ij}, is dependent on the nature of the adhesion molecules and antibodies mediating function, their concentration during cell activation, and the contact time between the aggregates during collision. For the lymphocyte systems discussed here, the avidity of activated cells was so high that most collisions resulted in adhesion. Under the conditions used for these experiments, we did not observe a dependency of the sticking probability on aggregate size, and in the subsequent discussion we will assume that P_{ij} is independent of aggregate size. This assumption, however, can easily be relaxed.

Cell-cell and cell-aggregate collision frequencies

The collision frequency, Z_{ij}, of cells migrating on a two-dimensional surface was found by adapting Smoluchowski's flocculation theory (Smoluchowski, 1917; Chandrasekhar, 1943; Overbeek, 1952). This theory is based on the fact that all aggregates of size i have a cylindrical region of influence of radius R_{ij} surrounding them. If any other aggregate with radius R_j comes within this region, the two will bind to form a single aggregate. The radius R_{ij} is the sum of the radius of the two individual aggregates $(R_i + R_j)$.

Consider a simple case in which a stationary cell is fixed at the origin of a large area in which similar cells are uniformly distributed at a concentration C_0 at time $t = 0$. The cells migrate on the surface, and when any of them enters this fixed cylindrical region of influence around the stationary cell with radius R_{ij}, it is "absorbed." We are interested in the flux of cells into this shell, because it will give us an expression for the collision frequency. The change in the cell concentration, C, in this field at any time t is found by solving Fick's diffusion equation:

$$\frac{\partial C}{\partial t} = D\nabla^2 C, \tag{9}$$

where D is the random motility coefficient of the cells in the uniform environment. If the experiment is carried out in a circular culture area of radius b, the initial and boundary conditions are

$$\begin{aligned} &C = C_0 && \text{at } t = 0 \text{ and } |r| > R_{ij} \\ &C = 0 && \text{at } t > 0 \text{ and } r = R_{ij} \\ &\partial C/\partial r = 0 && \text{at } t > 0 \text{ and } r = b. \end{aligned} \tag{10}$$

For these boundary conditions, the solution of the diffusion equation (presented by Eq. 11 below) gives the time and coordinate dependence of C (Carslaw and Jaeger, 1959; Adam and Delbrück, 1968):

$$C(r, t) = C_0\pi \sum_{n=1}^{\infty} \frac{[J_1(y_n)]^2}{[J_0(ky_n)]^2 - [J_1(y_n)]^2} e^{-Dy_n^2t/b^2} \bar{X}_0(r, y_n), \tag{11}$$

where

$$\bar{X}_0(r, y_n) = Y_0(y_n r/b)J_0(ky_n) - J_0(y_n r/b)Y_0(ky_n). \tag{12}$$

$J_n(y_n)$ and $Y_n(y_n)$ are Bessel functions of order n, and y_n are

the positive roots of

$$J_0(ky)Y_1(y) - Y_0(ky)J_1(y) = 0 \tag{13}$$

and

$$k = R_{ij}/b = \frac{R_i + R_j}{b}. \tag{14}$$

The flux into the cylindrical region at $r = R_{ij}$ is a measure of the total number of collisions that would take place with a stationary cell placed at the center of the well.

$$\text{Flux, } J = 2\pi aD \left.\frac{\partial C}{\partial r}\right|_{r=R_{ij}} = 4C_0\pi D \sum_{n=1}^{\infty} \frac{[J_1(y_n)]^2}{[J_0(ky_n)]^2 - [J_1(y_n)]^2} e^{-Dy_n^2 t/b^2}. \tag{15}$$

More generally, let us consider two types of aggregates of size i and j with random motility coefficients D_i and D_j. Since the motion of the aggregates is completely independent of each other, the effective random motility coefficient D_{ij} is

$$D_{ij} = D_i + D_j. \tag{16}$$

The number of collisions between the aggregates of size i and j, both diffusing in the uniform environment, follows immediately from Eq. 15 (Overbeek, 1952). The collision kernel evaluated by this approach is

$$k_{ij}C_iC_j = 4\pi D_{ij}C_iC_j \sum_{n=1}^{\infty} \frac{[J_1(y_n)]^2}{[J_0(ky_n)]^2 - [J_1(y_n)]^2} e^{-D_{ij}y_n^2 t/b^2} P_{ij}. \tag{17}$$

The kinetic rate constant for aggregation depends on the effective radius of collision (R_{ij}), the random motility coefficient of aggregates of size i (D_i), and the sticking probability (P_{ij}). The following sections focus on developing mathematical expressions for these parameters.

Effective radius of collision

The aggregate radius is an important parameter because it influences the effective radius of collision R_{ij} and, consequently, the collision frequency (Eq. 17). The radii R_i of the aggregates were calculated after correcting for their nonspherical shape. Our experiments with homotypic lymphocyte aggregation (Neelamegham et al., 1996) have shown that aggregates have morphologies that range from flat planar clumps with negligible vertical stacking to large, tightly packed aggregates with considerable vertical cell stacking (Fig. 1). Thus the effective radius of an aggregate depends not only on the number of cells it contains, but also on the extent of multilayered stacking.

Simple geometric arguments were applied to evaluate the effective collision radii of doublets and triplets (Eq. 18). Larger aggregates with more than three cells, however, form multilayered aggregates. The effective radius, R_i, of an aggregate of size i ($i > 3$) is based on the stacking index β (Eq. 1). It is given by

$$\frac{R_i}{R_1} = \begin{cases} 1 & i = 1 \\ 1 + i/\pi & i \le i \le 3 \\ \sqrt{i(1-\beta)} & i > 3. \end{cases} \tag{18}$$

Random motility coefficient of cells and cell aggregates

The random motility coefficients of cells and cell aggregates affect the rate of aggregation by influencing the collision frequency in Eq. 17. This coefficient can be measured experimentally for single cells by tracking the motion of the cells in a uniform environment under the light microscopy setup and by applying the persistent random-walk model (Dunn and Brown, 1987; Stokes et al., 1991) as described in the Experimental Methods section. Once this measurement is obtained, the "elementary force balance approach" proposed by Lauffenburger (1989) gives us a convenient way to estimate the random motility coefficients of cell aggregates.

The motion of cells has been described as a three-step process (Lauffenburger, 1989). During the first step there is a lamellipodium extension at the leading edge. This is followed by a second step in which the cell-substrate attachment at the anterior end causes a contractile force in the cell. Cell translocation requires an asymmetry in the cell-substrate interactions between the lamellipodium extension and the rear of the cell (DiMilla et al., 1991). This asymmetry may be caused by differences in the spatial distribution of cell surface adhesion receptors (Bretscher, 1984), or by spatial variations of cell receptor-ligand affinities between the front and the rear of the cell (Grinnell, 1986). As a result of this asymmetry in cell-substrate interactions, cell-substrate bonds at the posterior of the cell are being broken in preference to the bonds at the anterior, thus resulting in a net forward movement. If we model the motion of a cell as a continuous single-step process, the time-averaged force balance can be written (Lauffenburger, 1989) as

$$F_{drag} + F_{c-s} - F_l = 0, \tag{19}$$

where F_l is the contractile force acting on the lamellipodia that pulls the cells in the forward direction; F_{c-s} is the force due to cell-substrate attachment, which opposes this motion; and F_{drag} is the "frictional drag" due to the surrounding fluid. Because cell motion is slow and on a small length scale, one may assume a linear Stokes' resistance (F_{drag} = drag coefficient × cell speed) from the surrounding fluid. At low Reynolds numbers, the drag coefficient for a cell with radius R moving with a velocity v in a medium of viscosity μ can be approximated by

$$F_{drag} = 6\pi\mu Rv. \tag{20}$$

If we now use the subscript 1 to denote the properties of a single cell, the velocity v_1 of a single cell can be found by eliminating the frictional drag force from Eqs. 19 and 20:

$$v_1 = \frac{1}{6\pi\mu R_1}(F_e)_1 - (F_{c-s})_1). \tag{21}$$

The force balance approach is extended in the Appendix to derive an expression for the random motility coefficient of cell aggregates. As shown in Eq. A15, the random motility coefficient D_i of cell aggregates is a function of the random motility coefficient D_1 of single cells, the stacking index β, and the force asymmetry factor ξ, defined as

$$\xi = (F_i)_1/(F_{c-s})_1.$$

The factor ξ is based on the properties of a single cell and expresses the ratio of the contractile forces acting on the lamellipodium to induce locomotion over the cell-substrate adhesion forces at the rear of the cell that resist cell motion. Thus the asymmetry factor ξ is analogous to the parameter ψ, which DiMilla et al. (1991) used to describe the ratio of the uropodal to lamellipodal adhesivity. Whereas ψ is the ratio of the intrinsic dissociation rates of bonds at the rear and front of the cell, ξ is the ratio of the forces acting on the two ends. The force asymmetry factor provides a methodology by which we can scale up the behavior of single cells to predict the motility characteristics of larger aggregate. As shown in the Appendix (Eq. A15), ξ is an important parameter of the function describing the dependence of random motility coefficient of aggregates D_i on aggregate size i (see also Fig. 4). For a cell to be motile, the motility ratio must exceed unity and the random motility coefficient of large cell aggregates increases with increasing values of ξ.

Normalized form of the model equations

We now define normalized species concentrations C_{ij}* and time t* as well as four parameter groups to de-dimensionalize the ordinary differential equations of Eq. 6 describing the transient behavior of our aggregation system:

$$C_i^* = \frac{C_i}{C_0} \qquad P_{ij}^* = \frac{P_{ij}}{P_{11}}$$

$$t^* = \frac{D_1 t}{b^2} \qquad p_{ij}^* = \frac{k_{ij}}{P_{11}D_1} \tag{22}$$

$$D_{ij}^* = \frac{D_{ij}}{D_1} \qquad \alpha = \frac{1}{C_0 P_{11} b^2}.$$

Substituting these parameters into the collision kernel in Eq. 17, we obtain

$$k_{ij}^* C_i^* C_j^* = 4\pi D_{ij}^* C_i^* C_j^* \sum_{n=1}^{\infty} \frac{[J_1(y_n)]^2}{[J_0(ky_n)]^2 - [J_1(y_n)]^2} e^{-D_{ij}^* y_n^2 t^*} P_{ij}^*. \tag{23}$$

The ratio of Bessel functions in Eq. 23 is only a function of the aggregate sizes i, j and of the radius b of the culture area. If we denote this ratio by $g(i, j, b)$, the dimensionless model equation is

$$\alpha \frac{dC_i^*}{dt^*} = \frac{1}{2}\sum_{j=1}^{i-1} 4\pi D_{i-j,j}^* C_{i-j}^* C_j^* P_{i-j,j}^* \left(\sum_{n=1}^{\infty} g(i-j, j, b) e^{-D_{i-j,j}^* t^* y_n^2} \right) - \sum_{j=1}^{N_0-i} 4\pi D_{i,j}^* C_i^* C_j^* P_{i,j}^* \left(\sum_{n=1}^{\infty} g(i, j, b) e^{-D_{i,j}^* t^* y_n^2} \right) \tag{24}$$

$$\text{for} \quad \begin{matrix} i = 1, 2, 3 \ldots N_0 \\ j = 2, 3 \ldots N_0 \end{matrix}.$$

RESULTS AND DISCUSSION

Data analysis

The aggregation model was solved by numerically integrating the system of ordinary differential equations (Eq. 24) using the Runge-Kutta-Fehlberg (4, 5) algorithm (Fehlberg, 1970; Shampine et al., 1976). At each time point, the numerical solution of Eq. 24 gives the concentration of cell aggregates containing k cells, C_k, where $k = 1, 2, \ldots N_0$. From these data we first compute the cumulative size distribution given by

$$X_i = \sum_{k=1}^{i} \frac{k(C_k A_t)}{N_0}, \tag{25}$$

where X_i is the fraction of the cells associated with aggregates containing at most i cells. Our simulations start with nonaggregated cells, and thus the initial size distribution is a step function:

$$X_i = 1, \quad \text{for} \quad i = 1, 2, \ldots, N. \tag{26}$$

As aggregates of various sizes are formed, the cumulative size distribution curve widens and their mean moves to larger aggregate sizes. Fig. 2 *a* shows the temporal evolution of the cumulative size distribution curves obtained by integrating a system of 600 equations. All other parameter values are given in Table 1. As aggregation proceeds, these curves shift toward larger sizes, but the rate at which large aggregates form slows down. Although large aggregates sweep more area than small aggregates, aggregate motility decreases with size, resulting in fewer collisions and diminishing formation rates. Another reason for the decreasing aggregate formation rates is the disappearance of highly motile species. The model predicts that the number of nonaggregated cells or even aggregates with few cells decreases rapidly with time.

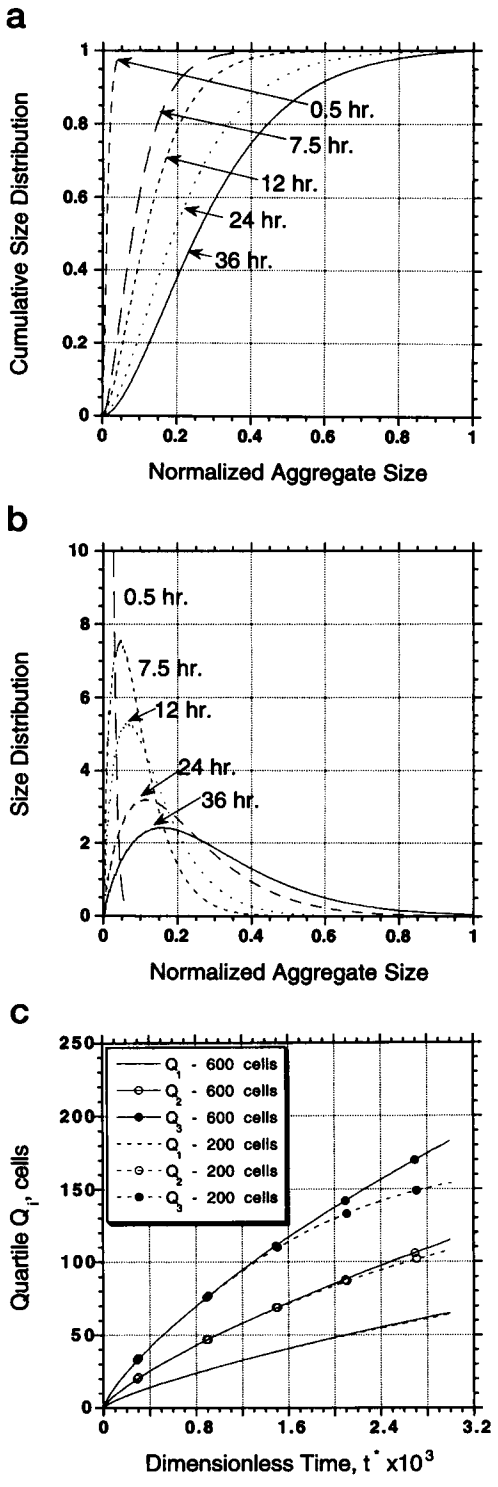

FIGURE 2 Aggregate size distributions. (*a*) Cumulative size distribution curves predicted by the aggregation model at various time points (0.5 h, 7.5 h, 12 h, 24 h, 36 h). Aggregate sizes are normalized with respect to the total number N_0 of equations solved (N_0 = 600). All other model parameter values are given in Table 1. (*b*) Size distribution curves predicted by the aggregation model at various time points (0.5 h, 7.5 h, 12 h, 24 h, 36 h). All model parameter values are given in Table 1, except N_0 = 600. (*c*) Quartile value plot comparing simulations solved with a total of 200 equations (*dashed lines*) and 600 equations (*solid lines*) show the temporal evolution of Q_1, Q_2, and Q_3. For these runs the dimensionless time t^* was given by $1.254 \times 10^{-4} \times t$.

TABLE 1 Reference values for aggregation model parameters

Number of equations	$N_0 = 200$
Force asymmetry factor	$\xi = 30$
Seeding density	$C_0 = 1700$ cells/mm^2
Stacking index	$\beta = 0.45$
Radius of single cell	$R_1 = 6.5$ μm
Binding probability	$P_{ij} = 0.83$ for all i and j
Random motility coeff.	$D_1 = 1{,}038$ μm^2/h
Radius of experimental well	$b = 2877$ μm

By differentiating the cumulative distribution curves, the size distribution curves of Fig. 2 *b* are obtained. Thirty minutes after the start of the experiment, the size distribution has a very narrow and tall peak, as most of the aggregates are still very small. As larger aggregates form, the size distribution spreads out and its maximum height decreases (see distribution at 7.5 h). Whereas the height of the size distribution falls rapidly at the start of the experiment, the aggregation process slows down because of the decreasing rates of formation of large aggregates.

The kinetics of aggregate formation may also be monitored in terms of the quartile values Q_1, Q_2, and Q_3 of the cumulative size distribution. Fig. 2 *c* shows the evolution of the quartile values for the simulation shown in Fig. 2, *a* and *b*. By plotting Q_1, Q_2, and Q_3 versus time, we can follow in one plot 1) the average aggregate size given by the Q_2 curve and 2) the width of the aggregate size distribution given by the interquartile distance $(Q_3 - Q_1)/Q_2$.

Effect of system parameters on predicted aggregation kinetics

The following is a list of the main model parameters:

A_t: Surface area of the two-dimensional closed system (i.e., bottom of tissue culture well) where cell aggregation takes place (μm^2).

N_0: Number of cells placed initially in the system.

β: Stacking index quantifying the vertical stacking in the cell aggregates (dimensionless). It can be measured by homotypic aggregation experiments.

D_1: Random motility coefficient of single cells (μm^2/h). It can be measured by independent motility experiments as described in the Experimental Methods section.

ξ: Force asymmetry factor (dimensionless). This parameter describes the dependence of motility on aggregate size and can be determined by independent motility experiments using Eq. A15 and measurements of cell and aggregate random motility coefficients as demonstrated in Fig. 4.

P_{ij}: Sticking probability, i.e., the probability that aggregates of size i and j will adhere on collision (dimensionless). The P_{ij}'s depend on the nature of the cell system being studied and the activation protocol employed. It can be easily measured experimentally under the conditions of the aggregation experiment, by identifying cell-cell collision events and calculating the fraction of these collisions that lead to adhesion.

Clearly, the area where aggregation takes place and the initial number of cells are known for all experiments. The remaining four parameters (β, D_1, ξ, and P_{ij}) can be measured by independent motility and adhesion experiments for each cell system and activation protocol. Thus the model developed here provides a tool by which we can predict the aggregation behavior of cell populations.

A systematic analysis was carried out to determine the effect of the model parameters on aggregation kinetics. Fig. 2 *c* demonstrates the effect of the total number N_0 of equations solved on model predictions. Both runs shown in Fig. 2 *c* start with the same cell density. The simulation with 600 equations is carried out in an area three times larger than the area used for the simulation with 200 equations. Model predictions show very similar aggregation patterns for up to 12 h (note that the dimensionless time is defined here by $t^* = (D_1/b^2) * t = 1.25 \times 10^{-4} * t$). At longer times, however, the model predictions are significantly different, because only the simulation with 600 equations allows the formation of aggregates having more than 200 cells. The experimental data presented in this paper monitor cellular aggregation for 8–10 h after activation. We found that a system with 200 equations was sufficient for comparing simulation predictions with experimental results.

The effect of force asymmetry factor, ξ, on the temporal evolution of the average aggregate size, Q_2 (i.e., the mean of the aggregate size distribution) is shown in Fig. 3 *a*. Increasing the value of ξ did not affect the initial aggregation kinetics when most of the cells were singlets or small aggregates. At longer times, however, the average aggregate size markedly increased with larger force asymmetry factors. For small values of ξ, the larger aggregates were less motile and, consequently, the frequency of cell-cell collisions is lower and the quartile curves become flat at a smaller time point.

The sticking probability and the cell seeding density affect the aggregation kinetics in a similar fashion by altering the dimensionless number α in Eq. 22. In the range that we tested the model, α appeared to be an important model parameter, and doubling its value causes the average aggregate size to decrease by 50% (Fig. 3 *b*). The model can thus be used as a useful tool to normalize the results from runs of homotypic aggregation experiments that were carried out at different cell seeding densities.

As expected, the predicted aggregation rates accelerated when the random motility diffusion coefficient, D_1, was increased (Fig. 3 *c*). In contrast to Fig. 3 *b*, however, the relationship between the random motility coefficient and the average aggregate size was not linear. The average aggregate size increased more rapidly with increasing D_1 when the value of the motility coefficient was low. At higher values of the random motility coefficient, the average aggregate size became less sensitive to changes in D_1. This is because the singlets and other small motile species disappear more rapidly when the random motility coefficient is high, leading to a rapid decrease in the frequency of collisions.

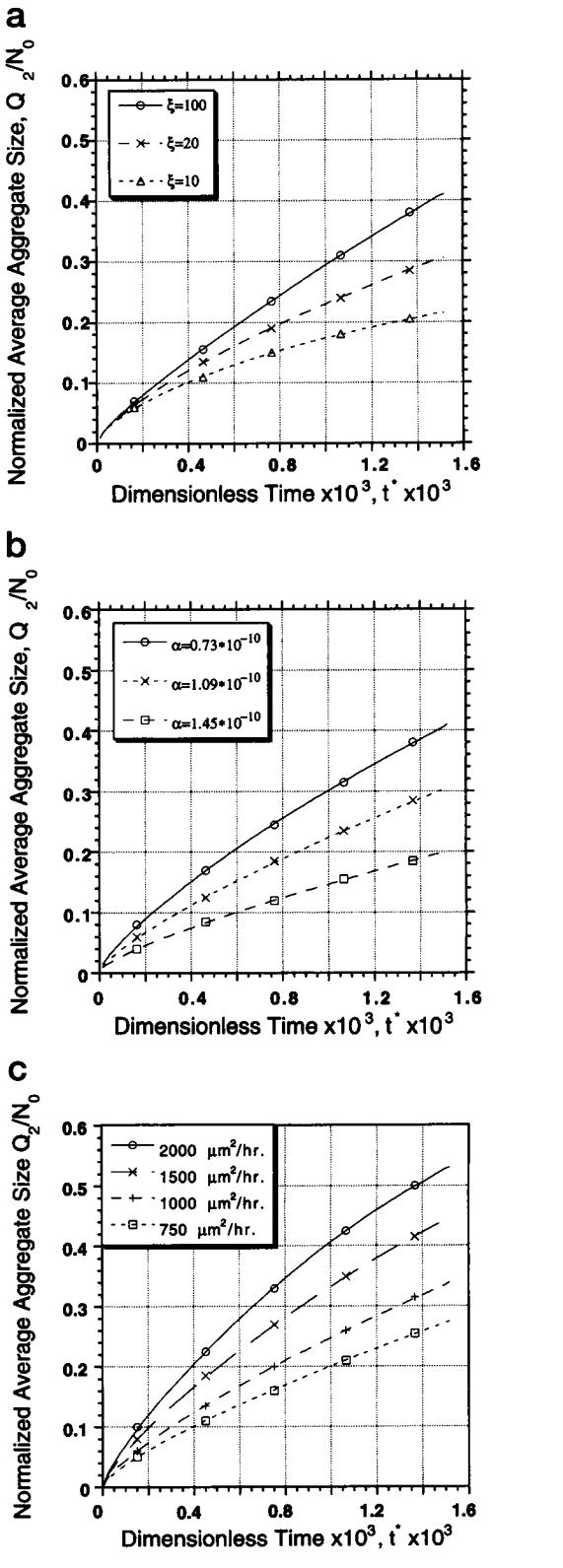

FIGURE 3 Effect of system parameters on aggregation rates. (*a*) Effect of force asymmetry factor ξ. (*b*) Effect of dimensionless number α defined in Eq. 22. (*c*) Effect of random motility coefficient D_1 of single cells. For all of these runs, the average aggregate sizes were normalized with respect to the total number of equations N_0 solved (N_0 = 200), and the dimensionless time t^* was $1.254 \times 10^{-4} \times t$. All other model parameters are given in Table 1.

The stacking index β and the experimental well radius b had very little effect on aggregation kinetics. Changing the stacking index from 0.0 (no cell stacking and consequently a larger collision radius) to 0.6 (compact aggregates with large vertical stacking) caused a decrease of less than 10% in the average aggregate size (data not shown). Similarly, doubling the well radius b caused a ~2% change in the average quartile value predicted (data not shown). Apparently the kinetics of aggregation are independent of the culture well radius b, and edge effects are negligible when the well radius is larger than 2877 μm (i.e., the radius of a 96-well plate).

Previous studies have speculated that not all cells have the same adhesion properties and that nonadhesive subpopulations of cells exist. These subpopulations may affect the kinetics of aggregation, as shown in Table 2. On decreasing the fraction of the adhesive cells in our system, we observe a larger decrease in the Q_1 and Q_2 values as compared to Q_3. Thus the width $(Q_3 - Q_1)/Q_2$ of the aggregate size distribution is larger in the presence of nonadhesive subpopulations, as compared to the distribution for cells with uniform adhesive properties (Table 2).

In summary, the singlet random motility coefficient D_1, the sticking probability P_{ij}, and the cell seeding density C_0 appear to be the important model parameters affecting the average aggregate size without changing the width of the aggregate size distribution. The width of the aggregate size distribution is determined by the nature of the cell system being studied and by the presence of cell subpopulations with different adhesive characteristics.

Comparison with experimental results

Homotypic aggregation of Jurkat cells was induced by the addition of monoclonal antibody to the β_1 integrin 33B6 as described earlier (Neelamegham et al., 1996). Induction of aggregation by this antibody is temperature dependent and requires ATP, divalent cations, and an intact cytoskeleton (Bednarczyk and McIntyre, 1990; Campanero et al., 1990; van de Wiel-van Kemenade et al., 1992). These requirements indicate that the observed aggregation is an active process rather than passive agglutination, where cells are cross-linked via bivalent antibodies. Such agglutination processes do not require energy and are not temperature dependent (Segal and Stephany, 1984).

The random motility coefficient of aggregates D_i depends primarily on two parameters: the force asymmetry factor, ξ, and the random motility coefficient of singlets, D_1. Whereas ξ depends on the cell type being studied, the random motility coefficient of singlets varies with the cell activation protocol and other experimental conditions. On activation with anti-β_1 antibody 33B6, the locomotion speed and root-mean-square speed of the cells decreased in comparison with a control experiment in which the cells were treated with OKT-11 mAb (Table 3). Although the persistence of cells treated with OKT-11 was not significantly different from that of cells activated with 33B6, the changes in the root-mean-square speed resulted in a dramatic decrease in the random motility coefficient of cells activated with 33B6 mAb (see Table 3).

As previously mentioned, the force asymmetry factor ξ is a scale-up parameter used to predict the random motility coefficient of cell aggregates from the behavior of single cells. Fig. 4 presents the change in the motility coefficients of aggregates predicted by Eq. A15 as a function of force asymmetry factor ξ and aggregate size i and compares them to experimental measurements. Almost all the experimental data quantifying the locomotion rates of Jurkat cell aggregates are consistent with an average value of the force asymmetry factor ξ equal to 30. Only the motility coefficient of the smallest aggregates with sizes between 20 and 40 cells was lower than that of larger aggregates. We attribute this behavior to the existence of subpopulation(s) of nonmotile cells that appear to have a lower force asymmetry factor, ξ. In our experiments with Jurkat cells, we found that ~10% of the aggregates remained stationary, and the size of most of these nonmotile species was in the 20–40 cell range. We expect that the nonmotile aggregates will have a smaller size, because they experience fewer cell collisions. Although a small subpopulation of cells may have a lower force asymmetry factor, an average value of $\xi = 30$ appears to provide an adequate description of the motility characteristics of a majority of the aggregates, and this will be the value used in subsequent comparisons with experimental data.

Fig. 5 *a* shows the aggregation kinetics for three runs carried out with the same number of cells but with different aggregation areas, resulting in different initial cell seeding densities. As expected, the runs with higher densities showed faster kinetics of aggregation. Simulation results agreed well with experimental measurements carried out

TABLE 2 Effect of cell adhesiveness on the spread of the aggregate size distribution

Fraction of adhering cells	Width of the aggregate size distribution	Average aggregate size, cells
1.0	1.05	61
0.9	1.2	51
0.8	1.66	41

TABLE 3 Effect of antibody addition on cell motility

Parameter	Control mAb, OKT-11	Anti-β_1 mAb, 33B6*
Number of cells observed	39	48
Avg. locomotion speed (μm/h)[§]	87.1 ± 11.6	52.1 ± 6.1
Root mean square speed (μm/h)[#]	63.4 ± 5.0	34.1 ± 1.7
Persistence time (min)[#]	26.5 ± 4.6	31.9 ± 3.7
Random motility coefficient ($\mu m^2 h^{-1}$)	885.1	307.9

*Concentration of anti-β_1 mAb, 33B6, corresponds to 80% site occupancy.
[#]Parameter values are reported with the asymptotic standard errors, which were calculated using the nonlinear regression procedure NLIN in SAS 6.07.02.
[§]Locomotion speed is reported along with SEM.

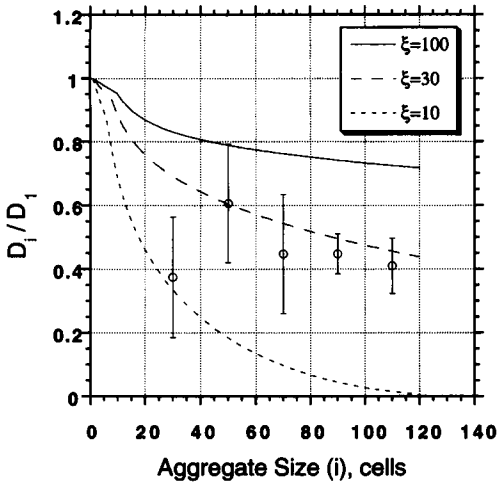

FIGURE 4 Force asymmetry factor. Predicted and measured random motility coefficients for cell aggregates are plotted as a function of aggregate size i for various values of the force asymmetry factor ξ. Open circles represent experimentally measured average random motility coefficients for aggregates in a given 20-cell size interval. Aggregates were grouped into intervals according to their size (20–40 cells, 40–60 cells, ... 100–120 cells), and the average random motility coefficient in each of these intervals was computed. Error bars represent SEM.

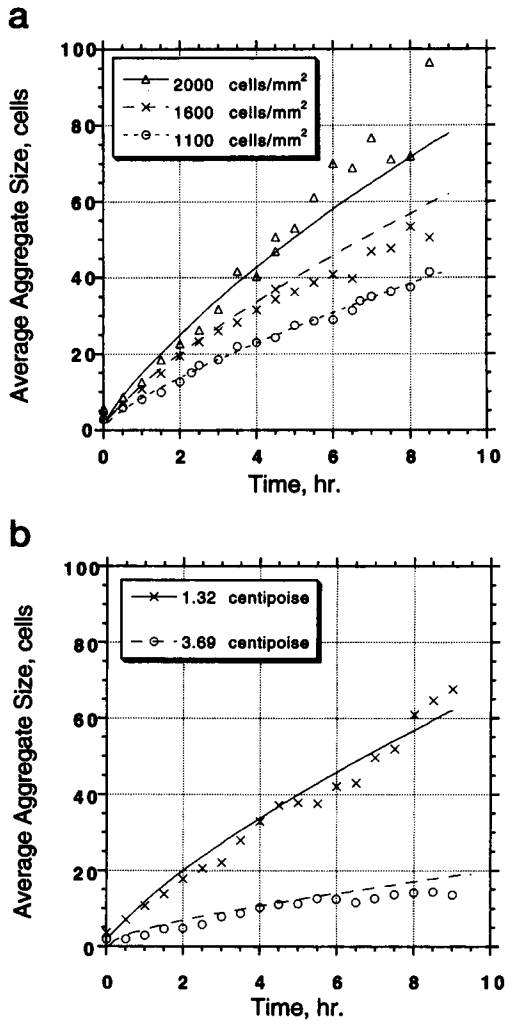

FIGURE 5 System parameters and rates of aggregation kinetics. (*a*) Experimental measurements (*symbols*) are compared to simulation predictions (*lines*) to determine the effect of cell seeding density on aggregation kinetics of Jurkat cells activated with 33B6. The concentration of 33B6 mAb corresponded to 80% site occupancy and the sticking probability P_{ij} was 0.97. (*b*) Effect of media viscosity on aggregation kinetics. Media viscosity was increased from 1.32 to 3.19 centipoise by addition of CMC, and the aggregation kinetics of Jurkat cells activated with 33B6 (80% occupancy) was monitored. For the model simulations (*lines*), D_1 for the higher viscosity media was set to 178 $\mu m^2/h$, and P_{ij} was 0.97. All other parameter values are given in Table 1.

with Jurkat cells activated by mAb 33B6 (corresponding to 80% site occupancy) at the same cell densities. Results indicate that in the range in which the experiments were performed, the average aggregate size increased linearly with increasing cell seeding densities.

Because the independent motility experiments were performed in media containing CMC, corrections were required for the increased drag, which resists cell motion under these conditions. To test the effect of increasing media viscosity on cell motility, CMC was added to the media at varying concentrations, and the random motility coefficient was measured as described in the Experimental Methods section. Upon increasing the media viscosity from 2.19 to 3.69 and 6.49 centipoise, the random motility coefficient decreased from 729 to 671 and 334 $\mu m^2/h$, respectively. These results confirm the hypothesis that the drag force experienced by the cells increased with increasing viscosity. For the sake of simplicity, we assumed that this relationship was linear, following Stokes' law (Eq. 20). Based on these studies, the random motility coefficient of cells cultured in regular media (not containing CMC) was estimated at 1038 $\mu m^2/h$ for cells activated with 33B6 mAb and 2983 $\mu m^2/h$ for cells on addition of OKT-11. These are the values of random motility coefficient used in the simulations (Table 1). To further test this modeling assumption, we performed aggregation experiments in media whose viscosity was increased through the addition of CMC. Fig. 5 *b* shows the effect of viscosity on the aggregation kinetics of Jurkat cells activated with 33B6. Increasing the media viscosity from 1.32 to 3.19 centipoise dramatically reduced the aggregation rate. We estimated that the higher viscosity decreased the random motility coefficient of Jurkat cells activated with 33B6 (corresponding to 80% site occupancy) from 1038 to 178 $\mu m^2/h$ as predicted by Stokes' law. This causes a ~5.8-fold decrease in the cell collision frequency and a consequent decrease in the rate of aggregation kinetics. As shown in Fig. 5 *b*, model predictions agreed well with the experimental results.

Fig. 6 compares the experimental and theoretical size distribution data at several time points for a typical experiment with Jurkat cells activated by mAb 33B6 corresponding to 30% site occupancy. To obtain the experimental data presented in these plots, we followed the aggregation kinetics of 3400 cells per digitized image. The stacking index

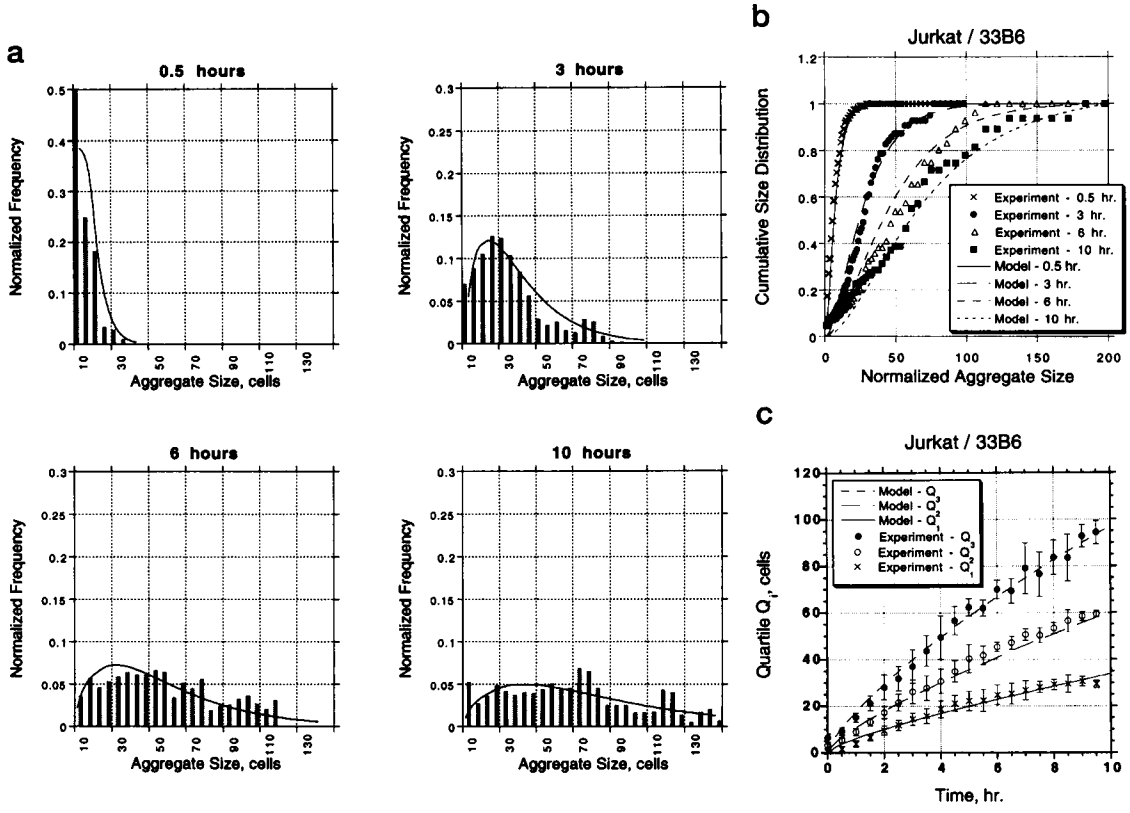

FIGURE 6 Aggregation kinetics of Jurkat cells incubated with 33B6. Jurkat cells were incubated with 33B6 at concentrations corresponding to 30% site occupancy, and their aggregation kinetics were monitored. Experimental data were compared with simulation predictions. All model parameters are given in Table 1. (*a*) Aggregate size distributions data at 0.5, 3, 6, and 10 h. The histograms represent the experimental results, and the smooth lines represent model predictions. (*b*) Cumulative size distributions at 0.5, 3, 6, and 10 h. (*c*) Experimental quartile data (*symbols*) are compared with model predictions (*smooth lines*). Error bars represent SEMs from three experiments.

was experimentally determined to be 0.45. The parameter values for these runs are listed in Table 1.

In the size distribution plots (Fig. 6 *a*) for Jurkat cells activated with 33B6, we observed a large number of singlets and small aggregates at 0.5 h. However, aggregation proceeded rapidly, leading to the formation of larger aggregates. Ten hours after the start of the experiment, the average aggregate size was about 60 cells, and several aggregates contained over 100 cells. The model did a very good job in predicting both the statistics of the aggregation population (Fig. 6, *a* and *b*) and the aggregation kinetics in the quartile plots (Fig. 6 *c*). The sticking probability for these simulations was 0.83, revealing that a very large fraction of the cell-cell collisions resulted in an adhesion event.

Fig. 7 compares the experimental results with simulation predictions when mAb OKT11 was added to the Jurkat cells. This mAb is a control antibody that does not induce aggregation of Jurkat cells beyond the level of spontaneous aggregation seen in the absence of any antibody. The random motility coefficient of the singlet for this simulation was 2983 $\mu m^2/h$, and the stacking index was equal to 0.1. The sticking probability estimated for this simulation was low ($P_{ij} = 0.07$), indicating that only a small fraction of the collisions resulted in adhesion. This demonstrates that aggregation kinetics is not only dependent on the rate of cell-cell collision, but also on the increased cell avidity as a result of cell activation. Although there is good agreement between the model and experimental data, indicating that the model is capable of capturing the features of the process even at very low avidity, we should note that the model predicts the complete disappearance of singlets, doublets, and smaller aggregates after a few hours. The experimental data, however, reveal that a fraction of the cells remain as singlets throughout the experiment, especially when the cells are not activated (Fig. 7). When nonadhesive cell subpopulations are present, therefore, the model will overestimate the Q_1 quartile values that are strongly affected by the presence of singlets and small aggregates.

Fig. 8 compares experimental results with model predictions to study the effect of mAb 33B6 dosage on aggregation kinetics. Simulations were performed in which the sticking probability P_{ij} was varied while keeping all other model parameters the same as in Table 1. In the absence of any antibody, the rate of aggregation was small and was limited by the sticking probability P_{ij} ($P_{ij} = 0.07$ in this case). On addition of 33B6 corresponding to 8% site occupancy, the sticking probability increased to 0.5, implying

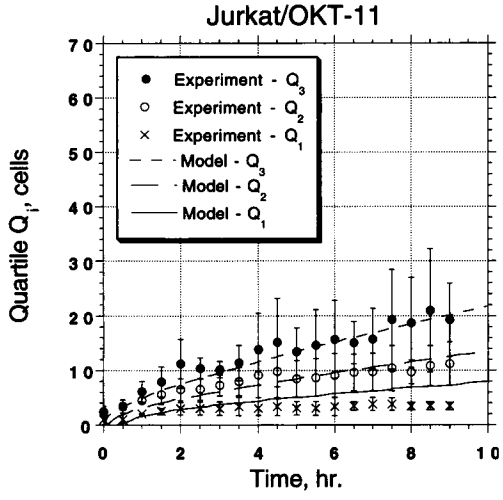

FIGURE 7 Aggregation kinetics of Jurkat cells incubated with OKT-11. Comparison of model predictions (*lines*) with experimental quartile values (*symbols*) for Jurkat cells incubated with the control antibody OKT-11 at a dilution of 1:500. Error bars represent SEM from three runs. For these experiments, $P_{ij} = 0.07$.

that the rate of aggregation was now controlled by both the random motility coefficient of the Jurkat cells and the sticking probability. Beyond mAb 33B6 concentrations corresponding to 30% occupancy, the sticking probability was greater than 0.83, and nearly all collisions resulted in adhesion. Here, aggregation kinetics was limited by the random motility coefficient of the cells. These results are consistent with our hypothesis that cell adhesion induced by antibodies to the β_1 integrin is a receptor-mediated phenomenon and that the avidity between the cells can be modulated by the dosage of 33B6 (Neelamegham et al., 1996). This hypothesis is also supported by our time-lapsed video observations, which showed that the binding efficiency reached its maximum at 30% 33B6 site occupancy, where most collisions resulted in adhesion between the colliding species.

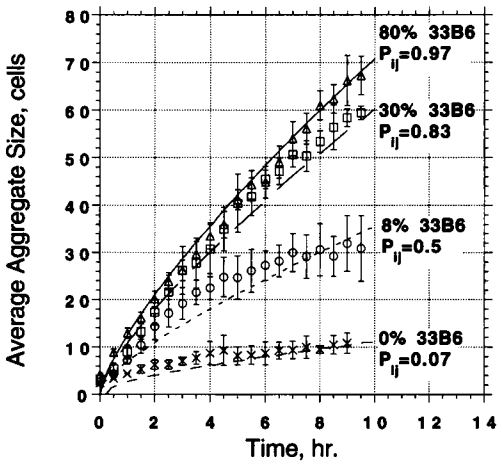

FIGURE 8 Effect of mAb dosage. Jurkat cells were incubated with various dosages of 33B6 (0%, 8%, 30%, 80% site occupancy), and the experimental results were fit to the model by changing the sticking probability P_{ij}. All other parameters are the same as in Table 1. Error bars represent SEMs from three experiments.

CONCLUDING REMARKS

The aggregation model presented here was able to accurately describe the temporal evolution patterns of the aggregate size distribution for several experimental conditions. It allowed us to analyze aggregation processes in terms of two groups of physical parameters: those describing the motility characteristics of cells or cell aggregates and those quantifying the adhesiveness or binding efficiency of cells. The model can also correct homotypic aggregation data for differences in initial cell densities among experiments, a common problem faced by immunologists working with this assay. Because cell motility can be independently quantified with direct measurements, the model can be used as a tool to evaluate the adhesiveness of activated cells using data from simple homotypic aggregation experiments performed under static conditions. Used in conjunction with currently available quantitative aggregation assays (Munn et al., 1993; Neelamegham et al., 1996; Neelamegham and Zygourakis, in press), this model has the potential to become a valuable tool for analysis of cell adhesion.

APPENDIX

Based on the "elementary force balance" approach, the velocity of cells and cell aggregates can be described in terms of the lamellipodia and cell-substrate adhesive forces (Eq. 21). Using the subscript 1 to denote singlets, the singlet velocity v_1 is

$$v_1 = \frac{1}{6\pi\mu R_1}(F_e)_1 - (F_{c-s})_1). \tag{A1}$$

In this paper the force balance approach was extended to predict the velocities and random motility coefficients of larger cell aggregates. For both the singlets and for larger aggregates, the force due to cell-substrate attachment is proportional to the number of bonds of attachment between the cell and the substrate. Assuming that receptor redistribution on the surface of the cells as a result of aggregate formation is not significant, this force is proportional to the surface area of contact between the aggregate and the substrate. Therefore, the force of attachment for a clump of i cells ($i > 3$), $(F_{c-s})_i$, as compared to the force of attachment of a singlet, $(F_{c-s})_1$, is given by

$$(F_{c-s})_i = i(1 - \beta)(F_{c-s})_1. \tag{A2}$$

The lamellipodia force of an aggregate is the vector sum of the lamellipodia forces of the individual cells comprising the base of the aggregate. Because the cells behave independently of each other, the net lamellipodia force of an aggregate with i' cells at its base is

$$(\vec{F}_l)_{i'} = (\vec{F}_l)_{1st\ cell} + (\vec{F}_l)_{2nd\ cell} + \ldots\ldots (\vec{F}_l)_{i'th\ cell}. \tag{A3}$$

For example, in the case of doublets, the net force in the lamellipodia can be calculated by the vector summation of the forces of two cells:

$$(\vec{F}_l)_2 = (\vec{F}_l)_{1st\ cell} + (\vec{F}_l)_{2nd\ cell}. \tag{A4}$$

If θ is the angle between the two forces, the expected value of the net

force $\langle F_l \rangle_2$ averaged over all possible values of θ is

$$\langle F_l \rangle_2 = \frac{(F_l)_1}{\pi} \int_0^{\pi} \sqrt{2}(\sqrt{1 + \cos\theta})\, d\theta = 1.27(F_l)_1. \quad \text{(A5)}$$

The net force between the cell and the substrate that resists motion doubles because the area of contact is twice that of a singlet. Substituting the individual forces into Eq. 21, we find an expression for the velocity of a doublet,

$$v_2 = \frac{1}{6\pi\mu R_2}(1.27(F_l)_1 - 2(F_{c-s})_1). \quad \text{(A6)}$$

Dividing Eq. A6 by Eq. A1,

$$\frac{v_2}{v_1} = \frac{R_1}{R_2}\left(\frac{1.27(F_l)_1 - 2(F_{c-s})_1}{(F_l)_1 - (F_{c-s})_1}\right). \quad \text{(A7)}$$

Applying the expression in Eq. 18 and substituting in the above equation, we get

$$v_2 = v_1\left(\frac{1}{1 + 2/\pi}\right)\left(\frac{1.27\xi - 2}{\xi - 1}\right). \quad \text{(A8)}$$

ξ is called the force asymmetry factor. It is the ratio of the lamellipodia force to the cell-substrate adhesion force in a single cell. This ratio allows us to vary the dependence of motility on aggregate size in accordance with experimental observations. The higher the value of ξ, the larger the random motility coefficient of cell aggregates. The velocity of an aggregate with three cells based on a similar analysis is

$$v_3 = v_1\left(\frac{1}{1 + 3/\pi}\right)\left(\frac{1.47\xi - 3}{\xi - 1}\right). \quad \text{(A9)}$$

The velocity expression for larger clumps ($i > 3$) is more complicated. Only the cells at the base of the aggregate contribute toward cell motion in these large, multilayered aggregates. Therefore, in a clump with i cells, $i(1 - \beta)$ cells contribute to the lamellipodia force. Let us denote $i(1 - \beta)$ by i'. The net lamellipodia force in a clump with i' cells touching the substrate is the vector sum of the forces of the net force in a clump of size $(i' - 1)$ and a singlet. The net lamellipodia forces of an aggregate with i' cells at its base equals the lamellipodia force of a singlet, $(F_l)_1$ times a constant $q_{i'}$ (Eq. A 10):

$$\langle F_l \rangle_i = q_{i'}(F_l)_1$$

$$= \frac{1}{2\pi}\int_0^{2\pi} \sqrt{((F_l)_1 + q_{i'-1}(F_l)_1\cos\theta)^2 + (q_{i'-1}(F_l)_1\sin\theta)^2}\, d\theta \quad \text{(A10)}$$

and

$$q_{i'} = \frac{1}{2\pi}\int_0^{2\pi} \sqrt{1 + q_{i'-1}^2 + 2q_{i'-1}\cos\theta}\, d\theta. \quad \text{(A11)}$$

Eq. A11 can be evaluated recursively with $q_1 = 1$ when $i' = 1$. Thus we derive an expression for the velocity of a clump with i cells ($i > 3$):

$$v_i = v_1 \frac{1}{\sqrt{i(1 - SI)}}\left(\frac{q_{i'}\xi - i(1 - SI)}{\xi - 1}\right) \quad \text{for } i > 3. \quad \text{(A12)}$$

Collating the expressions for the velocity of cell aggregates (Eqs. A6, A9, A12):

$$v_i = \begin{cases} v_1\left(\frac{1}{1 + 2/\pi}\right)\left(\frac{1.27\xi - 2}{\xi - 1}\right) & \text{for } i = 2 \\ v_1\left(\frac{1}{1 + 3/\pi}\right)\left(\frac{1.47\xi - 3}{\xi - 1}\right) & \text{for } i = 3, \\ v_1\frac{1}{\sqrt{i(1 - \beta)}}\left(\frac{q_{i'}\xi - i(1 - \beta)}{\xi - 1}\right) & \text{for } i > 3 \end{cases} \quad \text{(A13)}$$

where

$$q_{i'} = \frac{1}{2\pi}\int_0^{2\pi} \sqrt{1 + q_{i'-1}^2 + 2q_{i'-1}\cos\theta}\, d\theta \text{ and } q_1 = 1. \quad \text{(A14)}$$

The persistent random-walk model states that the random motility coefficient D is proportional to the square of the cell velocity v (Eq. 4) (Dunn and Brown, 1987; Stokes et al., 1991). As a first approximation, we assume that the persistence P of the aggregates is invariant with size. Thus from Eqs. A13 we derive an expression for the random motility coefficient for aggregates, D_i:

$$D_i = \begin{cases} D_1\left\{\frac{1.27\xi - 2}{(1 + 2/\pi)(\xi - 1)}\right\}^2 & \text{for } i = 2 \\ D_1\left\{\frac{1.47\xi - 3}{(1 + 3/\pi)(\xi - 1)}\right\}^2 & \text{for } i = 3. \\ D_1\left\{\frac{q_{i'}\xi - i(1 - \beta)}{\sqrt{i(1 - \beta)}(\xi - 1)}\right\}^2 & \text{for } i > 3 \end{cases} \quad \text{(A15)}$$

ACKNOWLEDGMENT

This material is partially based upon work supported by the National Aeronautics and Space Administration under award no. NAGW-5007.

REFERENCES

Adam, G., and M. Delbrück. 1968. Reduction of dimensionality in biological diffusion processes. In Structural Chemistry and Molecular Biology. A. Rich and N. Davidson, editors. W. H. Freeman and Company, San Francisco. 198–215.

Alt, W. 1980. Biased random walk models for chemotaxis and related diffusion approximations. *J. Math. Biol.* 9:147–177.

Bednarczyk, J. L., and B. W. McIntyre. 1990. A monoclonal antibody to VLA-4 α-chain (CDw49d) induces homotypic lymphocyte aggregation. *J. Immunol.* 144:777–784.

Bell, G. I. 1978. Models for the specific adhesion of cells to cells. *Science.* 200:618–627.

Bell, G. I. 1979. A theoretical model for adhesion between cells mediated by multivalent ligands. *Cell Biophys.* 1:133–147.

Bird, R. B., W. E. Steward, and E. N. Lightfoot. 1960. Transport Phenomenon. John Wiley and Sons, New York.

Botet, R., and R. Jullien. 1984. Size distribution of clusters in irreversible kinetic aggregation. *J. Phys. A. Math. Gen.* 17:2517–2530.

Bretscher, M. S. 1984. Endocytosis: relation to capping and cell locomotion. *Science.* 224:681–686.

Bretscher, M. S. 1987. How animal cells move. *Sci. Am.* 257:72–76, 89–90.

Campanero, M. R., R. Pulido, M. A. Ursa, M. Rodríguez-Moya, M. O. de Landázuri, and F. Sánchez-Madrid. 1990. An alternative leukocyte ho-

motypic adhesion mechanism, LFA-1/ICAM-1-independent, triggered through the human VLA-4 integrin. *J. Cell Biol.* 110:2157–2165.

Carslaw, H. S., and J. C. Jaeger. 1959. Conduction of Heat in Solids. Oxford University Press, London.

Chandrasekhar, S. 1943. Stochastic problems in physics and astronomy. *Rev. Mod. Phys.* 15:2–89.

Clayberger, C., A. M. Krensky, B. W. McIntyre, T. D. Koller, P. Parham, F. Brodsky, D. J. Linn, and E. L. Evans. 1987. Identification and characterization of two novel lymphocyte function-associated antigens, L24 and L25. *J. Immunol.* 138:1510–1514.

DiMilla, P. A., K. Barbee, and D. A. Lauffenburger. 1991. Mathematical model for the effects of adhesion and mechanics on cell migration speed. *Biophys. J.* 60:15–37.

Dolgosheina, E. B., A. Y. Karulin, and A. V. Bobylev. 1992. A kinetic model of the agglutination process. *Math. Biosci.* 109:1–10.

Doob, J. L. 1942. The Brownian movement and stochastic equations. *Ann. Math.* 43:351–369.

Dunn, G. A., and A. F. Brown. 1987. A unified approach to analysing cell motility. In Cell Behaviour: Shape, Adhesion and Motility. J. E. Heaysman, C. A. Middleton, and F. M. Watt, editors. The Company of Biologists Limited, Cambridge. 81–102.

Evans, C. W., and J. Proctor. 1978. A collision analysis of lymphoid cell aggregation. *J. Cell Sci.* 33:17–36.

Farrell, B. E., R. P. Daniele, and D. A. Lauffenburger. 1990. Quantitative relationship between single-cell and cell-population model parameters for chemosensory migration response of alveolar macrophages to C5a. *Cell Motil. Cytoskel.* 16:279–293.

Fehlberg, E. 1970. Klassische Runge-Kutta-formeln vieter und niedregerer ordnung mit schrittweitenkontrolle und ihre anwendung auf warmeleitungsprobleme. *Computing.* 6:61–71.

Freshney, R. I. 1987. Culture of Animal Cells: A Manual of Basic Technique. Wiley-Liss, New York.

Grinnell, F. 1986. Focal adhesion sites and the removal of substratum-bound fibronectin. *J. Cell Biol.* 103:2697–2706.

Hammer, D. A., and D. A. Lauffenburger. 1987. Dynamic model for receptor-mediated cell adhesion to surfaces. *Biophys. J.* 52:475–487.

Huang, P. Y., and J. D. Hellums. 1993. Aggregation and disaggregation kinetics of human blood platelets. Part I. development and validation of a population balance method. *Biophys. J.* 65:334–343.

Lauffenburger, D. 1989. A simple model for the effects of receptor-mediated cell-substratum adhesion on cell migration. *Chem. Eng. Sci.* 44:1903–1914.

Munn, L. L., M. W. Glacken, B. W. McIntyre, and K. Zygourakis. 1993. Analysis of lymphocyte aggregation using digital image analysis. *J. Immunol. Methods.* 166:11–25.

Neelamegham, S. 1995. The mechanism of homotypic aggregation of lymphocytes and motility characteristics induced by the activation of the β_1 integrin. Ph.D. thesis, Rice University.

Neelamegham, S., S. I. Simon, B. W. McIntyre, and K. Zygourakis. 1996. Induction of homotypic lymphocyte aggregation: evidence of a novel activation state of the β_1 integrin. *J. Leukocyte Biol.* 59:872–882.

Neelamegham, S., and K. Zygourakis. 1997. A quantitative assay for intercellular aggregation. *Ann. Biomed. Eng.* In press.

Nguyen, P. D., and E. A. O'Rear. 1990. Temporary aggregate size distribution from simulation of platelet aggregation and disaggregation. *Ann. Biomed. Eng.* 18:427–444.

Oster, G. F. 1984. On the crawling of cells. *J. Embryol. Exp. Morphol.* 83:329–364.

Overbeek, J. T. G. 1952. Kinetics of flocculation. In Colloid Science. H. R. Kruyt, editor. Elsevier Publishing Company, Amsterdam. 278–301.

Rothlein, R., and T. A. Springer. 1986. The requirement for lymphocyte function-associated antigen 1 in homotypic leukocyte adhesion stimulated by phorbol ester. *J. Exp. Med.* 163:1132–1148.

Samsel, R. W., and A. S. Perelson. 1982. Kinetics of rouleaux formation. I. A mass action approach with geometric features. *Biophys. J.* 37: 493–514.

Samsel, R. W., and A. S. Perelson. 1984. Kinetics of rouleaux formation. II. Reversible reactions. *Biophys. J.* 45:805–824.

Segal, D. M., and D. A. Stephany. 1984. The mechanism of intercellular aggregation: the kinetics of the Fcγ receptor-mediated aggregation of P388D1 cells with antibody-coated lymphocytes at 4°C. *J. Immunol.* 132:1924–1930.

Shampine, L. F., H. A. Watts, and S. M. Davenport. 1976. Solving non-stiff ordinary differential equations: the state of the art. *SIAM Rev.* 18: 376–441.

Smoluchowski, M. V. 1917. Versuch einer mathematischen theorie der koagulationskinetik kolloider lösungen. *Z. Phys. Chem.* 92:129–168.

Springer, T. A. 1995. Traffic signals on endothelium for lymphocyte recirculation and leukocyte emigration. *Annu. Rev. Physiol.* 57: 827–872.

Stokes, C. L., D. A. Lauffenburger, and S. K. Williams. 1991. Migration of individual microvessel endothelial cells: stochastic model and parameter measurement. *J. Cell Sci.* 99:419–430.

Sutherland, D. N., and I. Goodarx-nia. 1971. Floc simulation: the effect of collision sequence. *Chem. Eng. Sci.* 26:2071–2085.

van de Wiel-van Kemenade, E., Y. van Kooyk, A. J. de Boer, R. J. F. Huijbens, P. Weder, W. van de Kasteele, C. J. M. Melief, and C. G. Figdor. 1992. Adhesion of T and B lymphocytes to extracellular matrix and endothelial cells can be regulated through the β subunit of VLA. *J. Cell Biol.* 117:461–470.

Zeichner, G. R., and W. R. Schowalter. 1979. Effects of hydrodynamic and colloidal forces on the coagulation of dispersions. *J. Colloid Interface Sci.* 71:237–253.